On the Improvement of Cellular Coverage Maps by Filtering MDT Measurements

J. M. Sánchez-Martín, M. Toril, V. Wille, C. Gijón and M. Fernández-Navarro

Abstract—Cellular networks are constantly evolving, driven by changes in user behavior and device capabilities. To ensure that networks adapt to these changes, it is of vital importance for mobile operators to have a good understanding of how well their network meets subscriber needs. For this purpose, the Minimization of Drive Test (MDT) feature has been standardized, allowing operators the cost-effective provision of geolocated network performance statistics and radio events. However, in practice, positioning errors severely limit the potential of MDT measurements. In this paper, an in-depth analysis of a large MDT dataset taken from a commercial Long-Term Evolution (LTE) network shows for the first time several sources of positioning errors in MDT measurements not previously reported in the literature. To address these, a novel heuristic filtering algorithm is proposed to discard samples with inaccurate location data. Method assessment is done by checking the impact of filtering on the coverage map built with a real MDT dataset. Results show that the proposed filtering method significantly improves the accuracy of coverage maps by eliminating unreliable measurements.

Index Terms—MDT, positioning, LTE, coverage, GPS, tile, map, filter.

1 Introduction

Over the past years, cellular traffic has steadily increased driven by the introduction of smartphones and the increase in the average data volume per subscriber. In parallel, COVID-19 lockdown restrictions have shifted the geographical distribution of traffic demand from city centers to residential areas. As a result, some cells experienced very large increases in traffic, even when only a moderate traffic growth was observed across the whole network [1].

To cope with the above changing environment, cellular operators execute re-planning actions to redistribute traffic between neighbor cells (e.g., load balancing), add new network capabilities (e.g., large antenna arrays) or upgrade network resources (e.g., bandwidth extension, new carrier or new site) [2]. The potential impact of these actions is evaluated with radio network planning tools that estimate the expected network coverage and capacity with system performance models. Unfortunately, the increasing complexity of cellular networks makes it very difficult to capture system behavior with simple analytic models. In the absence of precise models, many of these tools use measurements from the live network to build empirical models.

Two valuable inputs for radio network planning are the real spatial user distribution and propagation conditions. Such information can be derived from measurements collected by geolocated user equipment. In the past, conventional drive test with specific test terminals provided pilot strength measurements, which were used to calibrate propagation models for outdoor and indoor scenarios. However, drive tests are time consuming, limiting the frequency and geographical coverage of these measurement campaigns [3]. To circumvent this limitation, 3GPP Release 10 standardized the Minimization of Drive Test (MDT) feature in order to automate measurement collection [4] [5]. MDT leverages User (i.e., subscriber) Equipment (UE) to collect field measurements combining radio performance and geo-location information.

Cellular positioning methods can be network-based, network-assisted, UE-based or UE-assisted approaches. In current LTE systems, the primary positioning method is Assisted GPS (A-GPS) [6], where the UE determines its location by processing GPS signals. For this purpose, a line-of-sight connection with several satellites and knowledge of orbital parameters are needed. Such data is downloaded before the first position fix, which can take several minutes for the first time (cold fix). To speed up that process, a network server can provide assistance data (e.g., accurate timing, satellite Doppler shift, coarse position of the mobile device or differential corrections) for a faster and more reliable GPS fix (warm fix). When GPS signal is not available (e.g., in urban or indoor environments), fallback positioning methods are used. In Enhanced Cell Identifier (ECID) [7] [8] [9], the UE reports the serving cell identifier, the radio link timing advance and serving/neighbor pilot signal level, from which a server approximates UE location. Alternatively, in Observed Time Difference of Arrival (O-TDOA) [10] the UE measures the time of arrival of positioning reference signals from multiple cells, from which a server derives user position by multilateration [11]. Moreover, the use of barometric sensors has recently been standardized for determining the floor level indoors [12]. The above techniques are complemented by other positioning schemes integrated in mobile operating systems such as fingerprinting/scene analysis [13], proximity sensing [14] and inertial sensors [15]. The reader is referred to recent surveys for a performance comparison of the different location techniques in indoor and outdoor scenarios [16].

- *J. M. Sánchez-Martín, M. Toril, C. Gijón and M. Fernández-Navarro are with Instituto de Telecomunicación (TELMA), Universidad de Málaga, CEI Andalucía TECH, E.T.S. Ingeniería de Telecomunicación, Bulevar Louis Pasteur 35, 29010 Malaga, Spain. E-mail: {jmsanchez, mtoril, cgm, mariano}@ic.uma.es*
- *V. Wille is with Nokia. Cambourne Business Park 1010, CB23 6DP Cambourne, UK. E-mail: volker.wille@nokia.com*

Manuscript received —- XX, 2021; revised —- XX, 20XX.

In parallel, mobile positioning techniques have improved, pushed by the success of location-based services [17]. Nowadays, mobile user location can be determined with a resolution of a few meters by combining legacy network-based schemes (e.g., cell identifier) with UE-based schemes relying on Global Navigation Satellite Systems (e.g., Global Positioning System, GPS) [11]. However, a major drawback of GPS receivers is their high energy consumption (up to 100 mW) [18] [19]. For this reason, modern mobile operating systems (e.g., Android and iOS) implement working modes that find the best trade-off between positioning accuracy and battery consumption [20] [21]. As a result, mobile devices only update their position when requested by an application or a significant change in location occurs [22]. As will be shown later, this behavior causes that location information in MDT measurements is inaccurate most of the time, which limits the value of these measurements for network operators.

In this work, a simple heuristic algorithm for filtering out MDT measurements with inaccurate (or outdated) location information is proposed. Firstly, a preliminary analysis of real MDT traces proves that energy saving schemes in handsets cause that the GPS receiver is only switched on intermittently. This fact leads in-accurate geo-location information in MDT reports. From the observation of real traces, a set of rules is derived to isolate those samples guaranteeing an adequate positioning accuracy. The input to the algorithm are common data fields in MDT reports. Method assessment is carried out with a large MDT measurement dataset taken from a commercial Long Term Evolution (LTE) network, by comparing the coverage map built with the original and the filtered samples.

The rest of the paper is structured as follows. Section 2 presents related work to highlight the contribution of this work. Section 3 introduces MDT measurements and describes the considered dataset. Section 4 formulates the problem of filtering MDT measurements. To this end, a preliminary analysis is carried out to unveil sources of inaccuracies in location information in MDT measurements. Section 5 outlines the proposed filtering algorithm for detecting MDT measurements with reliable location. Section 6 presents method assessment. Finally, Section 7 summarizes the main conclusions of the work.

2 Related work

Several works report the use of MDT measurements to build radio environment maps for cellular network optimization [23]. The concept was first introduced in [24], where a function is presented to process geolocated measurements reported by users to build radio performance maps (referred to as X-map). Later studies present direct methods that apply advanced interpolation techniques (e.g., inverse distance weighted [25] [26], nearest neighbors (NN) [27], splines [28] [25] or kriging [25] [29]) to build coverage, interference or signal quality maps from sparse MDT data reported by location-aware mobiles. Alternatively, indirect methods make use of regression techniques based on estimated or known parameters of the transmitter and radio propagation modeling (e.g., transmit power [30] or transmitter location [31]).

In all approaches, user position estimates are affected by the inaccuracies introduced by the wireless channel (e.g., non-line of sight, shadowing, multipath, etc.). Thus, several studies aim to characterize uncertainty due to these processes. In [32] [33], an analytical model is presented to estimate the impact of inaccurate user positioning due to GPS noise on cell edge and cell center coverage estimation. In [34], the impact of aggregating signal level measurements per map tile is evaluated. Then, an algorithm is proposed to estimate the optimal tile size for a given positioning accuracy and user density. In [35], an MDT database is used to characterize the geographical distribution of multipath effects and Doppler shift in cellular propagation channels. To reduce the impact of positioning errors, data filtering algorithms can be used, namely exponential smoothing, least-square methods [11], Bayesian filtering (e.g., Kalman filter [36] or particle filter [37]) and machine learning [38]. Some of these algorithms include dead reckoning techniques to predict the current position from past measurements of user direction/speed and elapsed time [15].

Most of the above-mentioned schemes to build coverage maps with MDT data were validated with simulated data, which might not reflect the true mechanisms behind MDT measurements. In the last years, handset vendors have introduced many functionalities to reduce battery consumption and keep user data privacy. It is known that these functionalities negatively affect the accuracy of positioning accuracy [39] [40]. However, to the authors' knowledge, no previous work has checked the impact of these functions on the accuracy of coverage maps built with MDT datasets. Likewise, no work has checked how widespread is the use of these features in real networks, in the absence of an official statement from vendors or a priori knowledge of how users set their terminals.

2.1 Contributions

In this work, a heuristic data filtering algorithm is proposed to discard samples with inaccurate location data measurements. Unlike the current practice in cellular network planning of treating each MDT measurement independently, the proposed filtering method relies on the construction of MDT traces. Moreover, unlike classical data filtering algorithms, the aim is not to reduce location errors due to GPS noise, but to detect abnormal states of the UE positioning system associated to energy saving and privacy modes. The main contributions of this work are: a) the disclosure of limitations on user location information in MDT data currently reported by handsets in different environments, b) a simple heuristic algorithm to filter out MDT measurements whose location information is not accurate and up-to-date due to abnormal UE positioning states, and c) an analysis of the impact of the above inaccuracies on the construction of coverage maps by direct methods over a recent MDT dataset taken from a live network.

3 MDT measurements and dataset

In this section, an introduction to MDT measurements is first presented. Then, the MDT dataset used in this work is described.

3.1 MDT measurements

Two MDT modes of operation can be configured in LTE: *immediate* and *logged*. The active mode is set on a per-tracking area basis. In immediate mode, MDT measurements are uploaded to the MDT server on the fly as long as a radio connection between the UE and the eNode B (eNB) is active. In logged mode, MDT information is measured and stored in the UE periodically (even in *IDLE* mode) during a certain logging duration, and data is then uploaded to the MDT server as 1 or more consecutive MDT reports when the UE switches to *CONNECTED* mode. The logging period is the maximum reported time that a UE can store location measurements and is typically set to 2 hours by network operators [41]. A longer collection window can be defined by combining measurement from multiple logging periods. Furthermore, the logging interval is defined as the time between samples that each UE stores in the scenario, often set to 1.28 seconds. Logging period and interval determine the amount of data reported per device on the network. The longer logging period and shorter interval, the larger number of measurements, and hence the higher location accuracy for moving users. The downside is a higher traffic volume in the radio interface caused by the MDT feature and higher computational load in network management tools.

Each MDT sample consists of about 70 predefined metrics, namely user and cell identifier, radio channel information (e.g., reference signal received power/quality), positioning information (e.g., latitude, longitude, altitude) or positioning accuracy (e.g., uncertainty ellipsoid, confidence), among others [42]. In logged mode, the large number of reported MDT samples (around 2 600 000 samples per UE and day) poses a storage and data processing problem (1 GB of data per day and cell in a suburban environment). To circumvent this issue, only a subset of relevant metrics is stored in the database.

3.2 Dataset

The MDT dataset considered in this work is obtained from a live LTE network. The dataset features are summarized in the table 1. In it, a site with three tri-sectorized cells is configured to store MDT reports in logged mode. Since UEs can store MDT measurements for up to 2 hours (in case the UE does not switch to connected mode for that time), some reports might include samples with serving cell different from the 3 cells collecting measurements if the user is highly mobile. For simplicity, the considered scenario is focused on the area covered by the main tri-sectorized eNB and the two nearest eNBs, covering 11.5 km^2 in a suburban area with 10 000 inhabitants. The carrier frequency of cells in the main eNB is 1 800 MHz, while neighbor eNBs use both 800 MHz and 1 800 MHz.

In the above described scenario, MDT reports are collected during 7 days. Thus, the dataset is consists of 7 files with a total of 15 069 214 samples from the selected eNBs (164 380 samples in the 800 MHz band and 14 904 834 in the 1 800 MHz band). For simplicity, the study is carried out over data from the 1 800 MHz band. To ease data storage and processing, the following features, reported on a per-measurement basis, have been stored for each MDT report:

LTE band	800 MHz / 1 800 MHz
MDT mode	Logged
Logging period	7 200 seconds
Logging interval	1.28 second
Area	11.5 km^2
Environment	Suburban/Rural
Duration	7 days
Number of samples	164 380 (800 MHz) / 14 904 834 (1 800 MHz)

TABLE 1: Features of the MDT dataset used in this work.

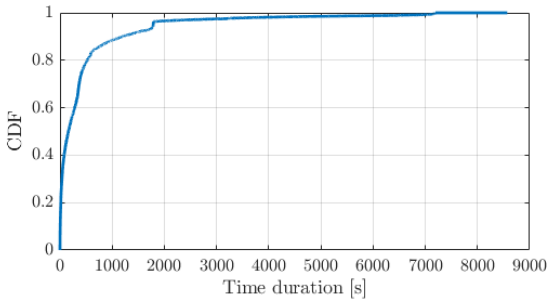

Fig. 1: Cumulative distribution function of MDT traces duration (61 327 traces).

1) MDT cell: cell where the MDT report is uploaded.
2) MDT upload time: timestamp of MDT report upload to the MDT server. The combination of upload time and C-RNTI is used to identify a MDT report from a specific UE univocally.
3) Serving cell: cell serving the UE when each measurement was taken.
4) Cell Radio Network Temporary Identifier (C-RNTI): temporary identifier used by an UE to upload data to the MDT server. C-RNTI is assigned at the end of the random access procedure and reassigned when the UE is inactive for a complete System Frame Number (SFN) cycle (i.e., 10.24 seconds) [43].
5) MDT time: timestamp indicating when each measurement in the MDT report was taken by the UE.
6) Longitude and latitude as position information.
7) Positioning accuracy, given by uncertainty and confidence [44]. Uncertainty is the length of the semi-major axis of the ellipsoid quantifying the location error. Confidence is paired with uncertainty and represents the probability with which a point is included within the error ellipsoid. For brevity, these features are hereafter referred to as uncertainty and confidence.
8) Reference Signal Received Power (RSRP) as a measure of radio channel conditions from the serving cell and its closest neighbor (if any).

From the complete dataset, 61 327 user mobility traces (hereafter referred to as MDT traces) are built by merging MDT reports with the same C-RNTI and serving cell in a temporal window of 2 hour maximum. By joining several consecutive reports from the same UE it is to obtain larger traces. Fig. 1 shows the resulting cumulative density function of trace length. It is observed that 6.5 % of traces are longer than 1 754 seconds ($\approx$ 30 minutes) comprising 47.5 % of the database due to huge amount of reports.

4 PROBLEM FORMULATION

In this section, a preliminary analysis over real traces is carried out to unveil sources of inaccuracies in location information in MDT measurements. Then, some design criteria for the filtering process are discussed.

4.1 Analysis of abnormal events in MDT traces

MDT traces allow checking the spatio-temporal evolution of UEs in the network. A comprehensive analysis has been carried out manually to detect abnormal events in MDT traces based on the above-described subset of features. The origin and impact of such events are discussed next.

4.1.1 Duplicate MDT reports

Some terminals upload the same information block to the MDT database twice. Fig. 2–(a) shows an example of duplicate blocks uploaded from the same UE with a short time difference. The first and third columns represent date and time for upload and measurements. In the first two columns, it is observed that the same UE (identified by C-NRTI) uploads the two blocks (highlighted in different colors) with a 434 ms difference. Specifically, the first block (green background) comprises information collected during 19 s (from 17:54:29 to 17:54:48) and uploaded at 19:20:26.597, whereas the second block (red background) comprises the same block of information but uploaded at 19:20:27.031. A more comprehensive analysis reflects that approximately 15% of samples in the dataset contain duplicate information. These duplicate reports from specific users unnecessarily increase the computational load and introduce bias on coverage statistics both at tile and network level.

4.1.2 Latitude rounding error

Some samples in MDT traces show the latitude field rounded to the lower sexagesimal degree. Such a rounding operation (only present in latitude) might be introduced by an obfuscation scheme due to the lack of permissions to access user location [45]. As a result, position is shifted tens of kilometers South/North, while longitude is still correct. To illustrate this phenomenon, Fig. 2–(b) represents the spatio-temporal evolution of positions in the trace of a static UE with rounded latitude error. Only latitude values are depicted for privacy reasons. By analyzing time values, it is observed that the trace consists of 5 consecutive periods where UE location switches between two distant points. A closer analysis shows that the latitude value of the point on the South has been rounded down to the lower integer. Such an undesirable effect, in this specific case, causes abrupt changes in user position of 25 km. These errors can be detected by checking decimals in the reported latitude value.

4.1.3 Defective positions

Detecting wrong samples without knowing the real UE position is a challenging task. Nonetheless, some reported positions show non-feasible mobility patterns far beyond the scope of the network. Such events appear in the trace shown in Fig. 2–(c), where some isolated positions spread around the globe are reported, whereas data come from users located in a European country. These outliers can easily be detected and eliminated by defining a bounding box based on coordinates of the country served by the network.

4.1.4 Dead reckoning

In high mobility traces, originated by UEs traveling in a vehicle (e.g., car or train), valid samples should be located on a road or railway track. However, mapping traces shows that the vehicle often follows a straight path finishing off the roads. Fig. 2–(d) shows a trace example of a UE inside a car on a motorway. It can be observed that, after some time on the road, the UE starts to describe a straight path for a few seconds. This event indicates signal loss or deactivation of positioning systems. Dead reckoning (a.k.a. inertial navigation) [46] is a relative positioning scheme that complements absolute positioning schemes when location reference signals are lost (e.g., indoors). It consists of inferring a new location/heading based on knowledge about movement speed and direction from a known starting point. In modern smartphones, movement is estimated by inertial sensors (e.g., accelerometer).

4.1.5 Intermittent reporting of positioning accuracy

The analysis of MDT traces shows that some UEs do not report any location accuracy information. As a result, 91.12% of MDT reports do not include any location accuracy information. This might be due to a reduced capability of GPS chipset. More interestingly, some UEs report location accuracy intermittently. For instance, Fig. 2–(e) shows the evolution of data in a trace from a quasi-static Android terminal. The light blue and red markers present the reported value of uncertainty and confidence, respectively. The deep blue markers depict the distance to the first location reported in the trace, computed using the Haversine formula (1)

$$d[n] = 2r * \arcsin\left(\sqrt{\sin^2(\tfrac{\phi[n]-\phi_0}{2}) + \cos\phi_0 \cos\phi[n] \sin^2(\tfrac{\lambda[n]-\lambda_0}{2})}\right) \quad (1)$$

where r is the Earth radius, λ_0 y ϕ_0 are the reference latitude and longitude respectively and, $\lambda[n]$ and $\phi[n]$ denote the latitude and longitude reported in sample n. Gaps in the distance curve point out the absence of location data for more than one second. After one minute, uncertainty and confidence data stop and a fixed location is reported until the next cycle. As will be discussed later, this behavior is due to energy saving modes in current mobile operating systems, where GPS is switched off most of the time to increase battery life. In particular, Android devices with Google Location Services enabled periodically report user location to Google servers [47]. Likewise, iOS devices maintain GPS off until apps request user location [22]).

4.2 Design principles

The above-described problems justify the need for filtering MDT measurements. Such a filtering can be formulated as a classification problem whose aim is to identify MDT samples with correct location data. The number of measurements in logged MDT databases is extremely large, since UEs are idle most of the time and measurements are registered on a second basis. Moreover, users tend to be static, causing MDT measurements to be highly redundant.

MDT UPLOAD	C-RNTI	MDT TIME	LATITUDE	LONGITUDE	RSRP
2019-07-25T19:20:26.597	60808	2019-07-25T17:54:29.000	52.347507	-0.35771012	-90
2019-07-25T19:20:26.597	60808	2019-07-25T17:54:30.000	52.347507	-0.35771012	-100
2019-07-25T19:20:26.597	60808	2019-07-25T17:54:32.000	52.347507	-0.35771012	-103
2019-07-25T19:20:26.597	60808	2019-07-25T17:54:33.000	52.347507	-0.35771012	-91
2019-07-25T19:20:26.597	60808	2019-07-25T17:54:34.000	52.347507	-0.35771012	-86
2019-07-25T19:20:26.597	60808	2019-07-25T17:54:36.000	52.347507	-0.35771012	-86
2019-07-25T19:20:26.597	60808	2019-07-25T17:54:37.000	52.347507	-0.35771012	-85
2019-07-25T19:20:26.597	60808	2019-07-25T17:54:38.000	52.347507	-0.35771012	-84
2019-07-25T19:20:26.597	60808	2019-07-25T17:54:39.000	52.347507	-0.35771012	-86
2019-07-25T19:20:26.597	60808	2019-07-25T17:54:41.000	52.347507	-0.35771012	-92
2019-07-25T19:20:26.597	60808	2019-07-25T17:54:42.000	52.347507	-0.35771012	-89
2019-07-25T19:20:26.597	60808	2019-07-25T17:54:43.000	52.347507	-0.35771012	-95
2019-07-25T19:20:26.597	60808	2019-07-25T17:54:45.000	52.347507	-0.35771012	-98
2019-07-25T19:20:26.597	60808	2019-07-25T17:54:46.000	52.347507	-0.35771012	-100
2019-07-25T19:20:26.597	60808	2019-07-25T17:54:47.000	52.347507	-0.35771012	-103
2019-07-25T19:20:26.597	60808	2019-07-25T17:54:48.000	52.347507	-0.35771012	-106
2019-07-25T19:20:26.597	60808	2019-07-25T17:54:50.000	52.347507	-0.35771012	-111
2019-07-25T19:20:26.597	60808	2019-07-25T17:54:51.000	52.347507	-0.35771012	-109
2019-07-25T19:20:26.597	60808	2019-07-25T17:54:52.000	52.347507	-0.35771012	-105
2019-07-25T19:20:27.031	60808	2019-07-25T17:54:29.000	52.347507	-0.35771012	-90
2019-07-25T19:20:27.031	60808	2019-07-25T17:54:30.000	52.347507	-0.35771012	-100
2019-07-25T19:20:27.031	60808	2019-07-25T17:54:32.000	52.347507	-0.35771012	-103
2019-07-25T19:20:27.031	60808	2019-07-25T17:54:33.000	52.347507	-0.35771012	-91
2019-07-25T19:20:27.031	60808	2019-07-25T17:54:34.000	52.347507	-0.35771012	-86
2019-07-25T19:20:27.031	60808	2019-07-25T17:54:36.000	52.347507	-0.35771012	-86
2019-07-25T19:20:27.031	60808	2019-07-25T17:54:37.000	52.347507	-0.35771012	-85
2019-07-25T19:20:27.031	60808	2019-07-25T17:54:38.000	52.347507	-0.35771012	-84
2019-07-25T19:20:27.031	60808	2019-07-25T17:54:39.000	52.347507	-0.35771012	-86
2019-07-25T19:20:27.031	60808	2019-07-25T17:54:41.000	52.347507	-0.35771012	-92
2019-07-25T19:20:27.031	60808	2019-07-25T17:54:42.000	52.347507	-0.35771012	-89
2019-07-25T19:20:27.031	60808	2019-07-25T17:54:43.000	52.347507	-0.35771012	-95
2019-07-25T19:20:27.031	60808	2019-07-25T17:54:45.000	52.347507	-0.35771012	-98
2019-07-25T19:20:27.031	60808	2019-07-25T17:54:46.000	52.347507	-0.35771012	-100
2019-07-25T19:20:27.031	60808	2019-07-25T17:54:47.000	52.347507	-0.35771012	-103
2019-07-25T19:20:27.031	60808	2019-07-25T17:54:48.000	52.347507	-0.35771012	-106
2019-07-25T19:20:27.031	60808	2019-07-25T17:54:50.000	52.347507	-0.35771012	-111
2019-07-25T19:20:27.031	60808	2019-07-25T17:54:51.000	52.347507	-0.35771012	-109
2019-07-25T19:20:27.031	60808	2019-07-25T17:54:52.000	52.347507	-0.35771012	-105

(a) Duplicate reports in the original MDT database.

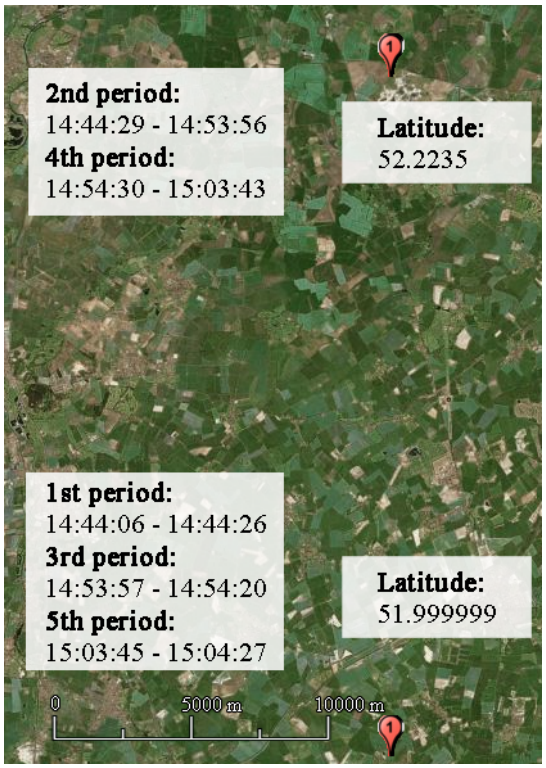

(b) Apparent changes in user latitude due to rounding errors.

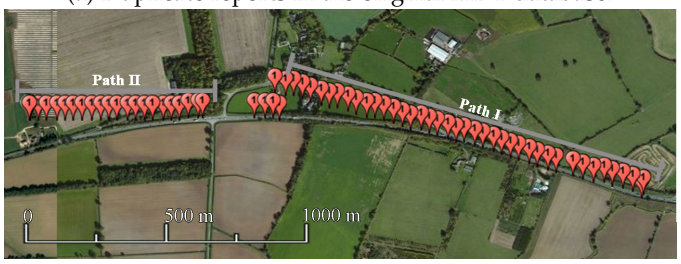

(c) User position offset due to dead reckoning.

(d) Defective positions reported by a single UE.

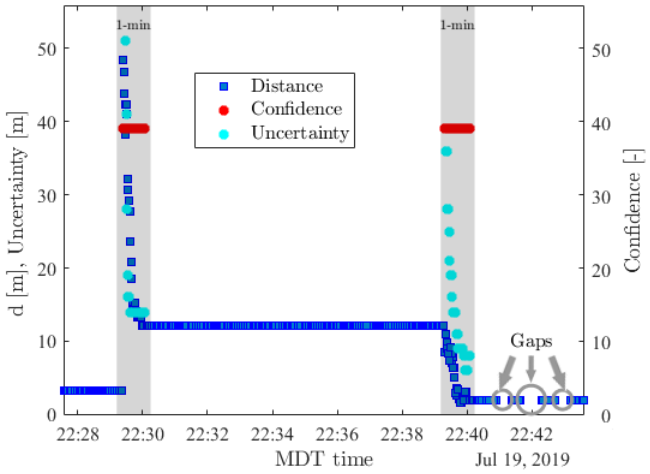

(e) Intermittent reporting of positioning accuracy information and convergence of uncertainty value.

Fig. 2: Abnormal positioning events detected in the preliminary analysis of MDT traces.

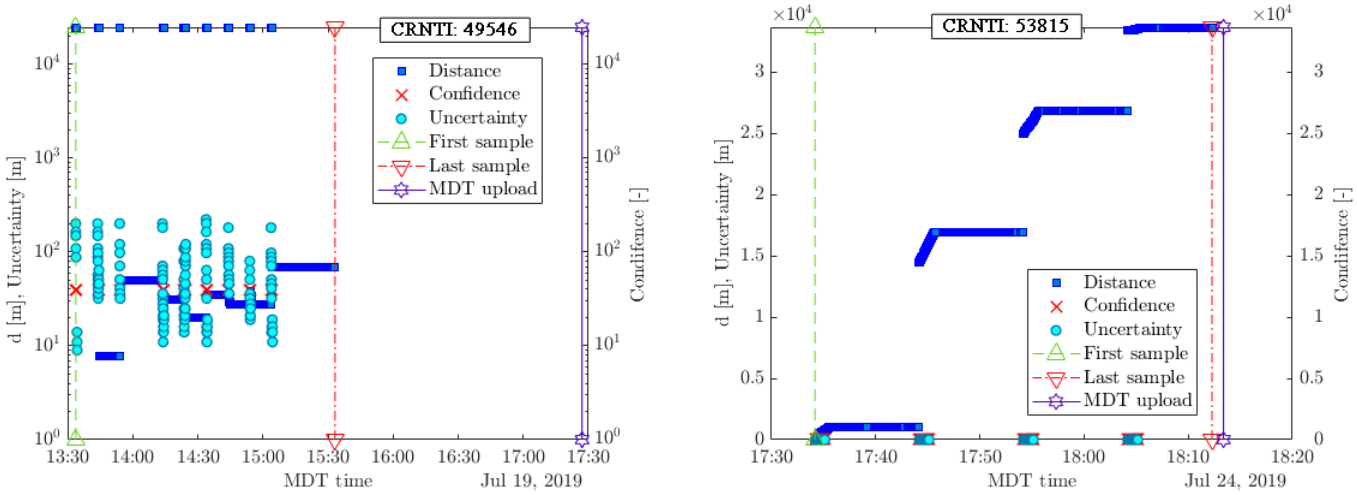

(a) Static device with rounded latitude and intermittent positioning accuracy event.

(b) Dynamic device traveling inside a car with intermittent positioning accuracy and dead reckoning event.

Fig. 3: Evolution of distance from the initial point (blue squares) and relevant events in two real MDT traces.

This property can be used to design restrictive filtering algorithms that strengthen the criteria fulfilled by a location measurement to be tagged as accurate. Thus, algorithms might discard correct measurements, as long as they discard incorrect ones. Yet, the number of output measurements must be large enough to ensure that important regions of the map are covered properly. This requirement is satisfied when the number of measurements per map tile is enough to ensure robust performance estimates. Thus, an important figure of merit of any MDT filtering algorithm is the average number of output samples per map tile and the size of confidence intervals for indicators derived per tile from MDT measurements.

Another important figure of merit is the computational load. Current filtering approaches are based on processing individual MDT measurements for simplicity. However, the number of samples discarded by these methods is small. More sophisticated algorithms can exploit the time dependence between features in user mobility traces to identify correct location measurements. However, complex operations with location data should be avoided for the sake of efficiency.

5 Heuristic Filtering Algorithm

In this section, a novel algorithm is presented to detect MDT measurements with correct positioning data. Unlike current approaches that treat data on a sample-by-sample basis, the proposed algorithm relies on user mobility traces to infer states of the UE positioning system. Filtering principles are derived from rules aiming to identify the different stages of the handsets. For this reason, trace analysis is first presented to illustrate the rationale of the algorithm. Then, the workflow of the algorithm is outlined.

5.1 Rationale of the algorithm

The proposed algorithm tackles the problem of classifying MDT measurements with heuristic rules derived from the analysis of real MDT traces. The analysis of these traces shows a cyclical pattern in many of them.

Fig. 3–(a) presents a long trace from a static UE. The analyzed MDT report, comprising 2 hours of measurements, is uploaded at 17:27:07, when the mobile identified by C-RNTI 49546 enters connected mode. In the idle period from 13:33:47 to 15:33:15, it is observed that uncertainty and confidence tends to be reported periodically every 10 minutes. As stated above, this behavior is due to energy saving mode. In particular, the trace comprises 9 measurement cycles. In most of them, the device reports uncertainty and confidence for 1 minute and then stops for the next 9 minutes. This is explained by the fact that Android devices with Google Location Services report user location every 10 minutes, which coincides with the period observed in Fig. 3–(a). A closer inspection of Fig. 2–(e) shows that uncertainty data, when reported, shows a convergence period, where its value progressively decreases. Such a period lasts for 1 minute, which is the typical time-to-first-fix in a warm start with A-GPS [48]. For this reason, this period is hereafter referred to as GPS acquisition period.

From the large distance values observed in the upper part of Fig. 3–(a), it can be inferred that latitude reported by the UE at the acquisition period is rounded to the nearest integer for privacy reasons. This behavior has been observed in many UEs. Immediately after, a valid position is reported, which is maintained for the next 9 minutes, reducing the number of valid measurements. Note that, even if a different valid position is reported in each measurement cycle, the distance between the reported locations is small. This fact suggests that the user might be static and those differences might be due to GPS location errors.

To confirm the cyclical pattern observed in static UEs, the analysis is now focused on dynamic UEs, that travel several kilometers within an information block. Fig. 3–(b), depicts an MDT trace of a dynamic UE traveling 33.68 km in 38 minutes. The trace comprises 4 cycles with the above-described stages. Every 10 minutes, the device reports uncertainty and

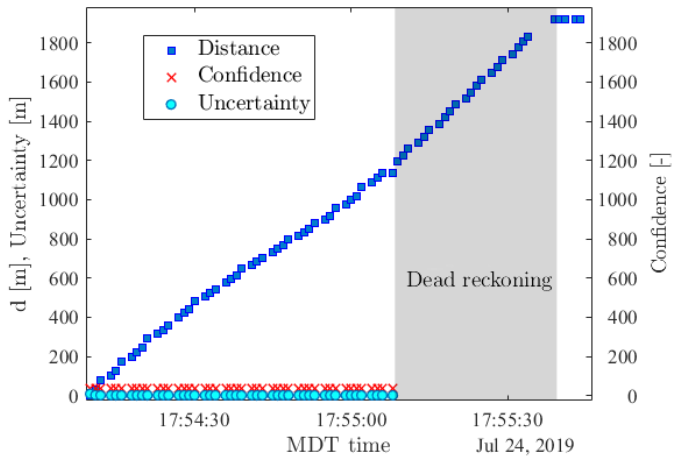

(a) Dynamic trace reporting up-to-date position and dead reckoning effect.

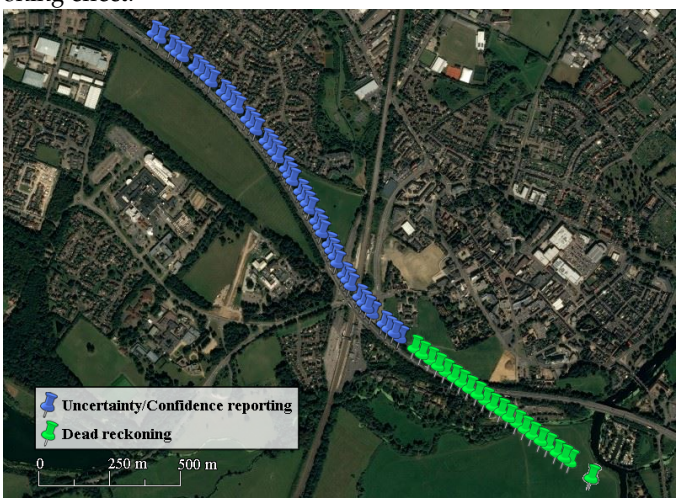

(b) Orthophoto.

Fig. 4: Graphical representation of a moving user (dynamic trace) including up-to-date position and dead reckoning effect.

confidence data for 1 minute approximately. During this period reported positions follow the road. Then, a straight path is observed due to dead reckoning. Dead reckoning works for some time (typically 30 seconds), after which the reported location remains fixed (in most cases off the road). Finally, the cycle starts again 8.5 minutes later with valid positions on top of the road. A closer analysis reveals that the start of dead reckoning, in most cases, coincides with the interruption of uncertainty/confidence reporting. Fig. 4 present a relevant example of this phenomenon. Fig. 4–(a) presents a trace from a user traveling at high speed (referred to in the text as dynamic trace). Fig. 4–(a) shows the values of distance (measured from the initial point, defined by the first valid location reported in the trace), uncertainty and confidence evolving with time. It can be noticed that the UE first reports the uncertainty and confidence values (hence, his/her handset has a GPS chipset that provides that information) and then stops doing so. Fig. 4–(b) shows the orthophoto of the trace. Blue markers represent samples reporting uncertainty and confidence, while green markers represent the remaining ones. By looking at green markers, it seems that the UE leaves the road following a straight path. Such a behavior suggests that the UE is in a period of dead reckoning. This effect of reporting uncertainty/confidence and then going through a dead reckoning state has been observed in many traces from dynamic users in the dataset. it is demonstrated the start of the dead-reckoning effect is usually derived from the end of report of the accuracy position measurements. This suggests that GPS is deactivated at the end of the acquisition period. However, in traces where GPS acquisition is shorter than 1 minute, it has also been observed that the next reported positions (until 1 minute) still follow the road accurately. This fact suggests that, in UEs with a cyclical reporting pattern, GPS is activated for at least 1 minute, even if uncertainty/confidence may be reported for a shorter interval if GPS acquisition takes less time. These samples shortly after the GPS acquisition period, obtained while GPS is in tracking mode, provide the most accurate location information. It has also been confirmed that every cycle has at least 1 correct sample at the end of the GPS acquisition period.

The above-described examples are representative of the typical behavior of MDT traces. From those findings, it can be concluded that: a) location data in MDT measurements is outdated (=inaccurate) most of the time, and b) uncertainty/confidence data can be used to isolate accurate location samples. Both principles are used in the algorithm proposed next.

5.2 Algorithm outline

The algorithm consists of three stages: data pre-processing, trace construction and sample classification.

5.2.1 Data pre-processing

The process starts by eliminating duplicate MDT reports by identifying samples with the same serving cell, C-RNTI and upload time. Likewise, MDT samples with defective position are detected and discarded by defining a bounding box based on the expected geographical area covered by the network. Then, the subset of features described in section 3.2 is selected to reduce storage and computational requirements.

5.2.2 Trace construction

Individual MDT traces are built by merging consecutive MDT reports uploaded in the same cell with the same C-RNTI. As a result, the time period covered by a trace can span from a few seconds up to several hours, depending on the last time the UE entered connected mode.

5.2.3 Sample classification

Fig. 5 shows the workflow of the algorithm. It is observed that each sample is classified into one of the following groups, based on reporting events and stages described in section 4.1:

1) Rounded: samples with rounded (i.e., wrong) latitude value.
2) Non-convergent acquisition: samples including accuracy information, but with uncertainty value

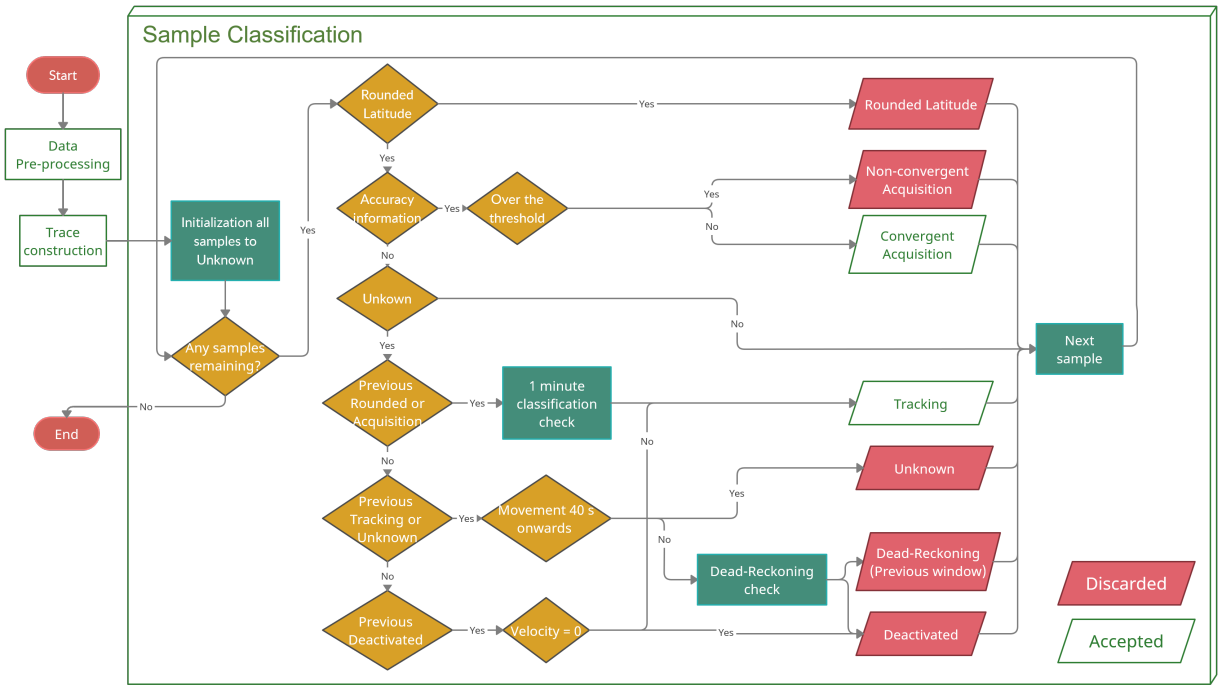

Fig. 5: Workflow of the proposed filtering algorithm, including internal classification rules and output labels.

larger than the above threshold. Position reported in these samples is considered to have an unacceptable error. This condition could be relaxed (e.g., by increasing the threshold) in an attempt to repopulate tiles without samples at the expense of a lower accuracy.

3) Convergent acquisition: samples including positioning accuracy information where uncertainty is below a certain threshold (in this work, 20 m). Position reported in these samples is considered to have an acceptable error.
4) Tracking: samples reported at the end of the acquisition stage (identified by the interruption of uncertainty/confidence measurements), which should report valid positioning information.
5) Unknown: this group includes a) samples not belonging to any of the previous groups in traces that include uncertainty/confidence measurements, and b) samples in MDT traces that do not include uncertainty/confidence measurements, where it is not possible to identify the acquisition and tracking stages of the GPS receiver.
6) Dead reckoning: samples describing a straight path during a minimum of 30 s. Position reported in these samples is considered to be invalid, as it cannot be guaranteed to be up to date for high mobility users.
7) Deactivated: contiguous samples when position remains fixed for a long period (e.g., 9 minutes), suggesting that GPS receiver is disconnected.

To classify samples, the algorithm analyzes each MDT trace sequentially. All samples are initialized to *unknown*. To start with, the algorithm searches for the first sample either with rounded latitude or including positioning accuracy information. Both conditions indicate the start of the GPS acquisition period in mobiles with a cyclical reporting pattern (rounded latitude for mobiles unable to report positioning accuracy due to privacy issues, start of confidence/uncertainty for mobiles with chipsets that can provide that information). In case of rounded latitude, the following samples with rounded latitude are also labeled as rounded, until the first sample with normal latitude is detected. In case of first uncertainty/confidence value, the following samples with that information are classified as *convergent acquisition* if uncertainty is below the predefined threshold, and *non-convergent acquisition* otherwise. This process follows until the first sample with no accuracy information is detected (end of GPS acquisition). If that sample is more than 1 minute after the start of the cycle, it is assumed that GPS is deactivated at the end of the GPS acquisition period, and only this sample is classified as *tracking*. In contrast, if that sample is more than 1 minute after the initial sample of the cycle, and the previous sample is tagged as *convergent*, the next samples until 1 minute are classified as *tracking*, to reflect the longer GPS tracking period. Once GPS deactivation is identified, the algorithm searches for a sufficiently long period (at least, 40 seconds) when location is fixed. Once detected, the algorithm processes the trace backwards, to check if the preceding samples in the last 30 seconds reflect any dead reckoning effect. For this purpose, the instantaneous UE speed is estimated from distance and time between consecutive samples. Successive samples with the same speed in this 30-second period are classified as *dead reckoning*. Then, following samples with exactly the same position are classified as *Deactivated*.

Only samples belonging to *convergent acquisition* and *tracking* groups are considered valid. Thus, once classification is performed, data samples classified as *unknown*, *rounded latitude*, *non-convergent acquisition*, *dead-reckoning* are

discarded, whereas samples classified as *convergent acquisition* and *tracking* are accepted.

6 Performance assessment

This section presents the results obtained by the proposed filtering algorithm over the dataset described in section 3.2. Analysis set-up is described first and results are presented later.

6.1 Experimental set-up

For computational efficiency, the proposed algorithm is implemented in different programming languages. Data preprocessing is carried out in Python with Pandas [49] and Numpy [50] libraries, used for data manipulation and numerical calculation, respectively. Then, measurement classification and filtering and the representation of traces in maps is carried out in MATLAB environment using the Mapping Toolbox [51].

It should be pointed out that building ground truth data would require a comprehensive measurement campaign with different handsets available in the market, as positioning reporting schemes largely vary between vendors. Such an approach would not reflect the actual share of different operative systems, terminals and user settings in the network. For this reason, in the absence of ground truth, method assessment is done by checking the consistency of the original and filtered coverage maps on a dataset taken from a commercial network.

Preliminary analysis breaks down the execution of the algorithm over 2 MDT traces. This experiment aims to analyze the filtering performed by the proposed algorithm on 2 MDT traces. Trace 1 is shown in Fig. 3–(b), belonging to a high-mobility user. Specifically, a 10-minute period of the trace is analyzed in this experiment, comprising 424 samples from the complete trace of 1625 samples. Trace 2 is shown in Fig. 3–(a), belonging to a static UE. In this case, the whole trace is analyzed, including 4374 samples collected during 120 min. Results are analyzed by representing positioning data on the globe via orthophotos.

Subsequently, a comprehensive analysis is performed to show the benefit of the proposed filtering algorithm in the automated construction of coverage maps. To this end, the algorithm is applied over a complete dataset of 61 327 MDT traces, comprising 18 363 186 measurement samples. Focusing on the studied area, a total of 15 069 214 samples are obtained from the original dataset. A preliminary analysis (not included here) shows that RSRP measurements in a tile tend to be *Student's T* distributed both before and after the filtering process.

The impact of filtering is analyzed by constructing 3 different maps for the original and filtered datasets:

1) Density map: map showing the number of samples per tile, this is used to detect the most crowded areas.
2) Coverage map: map representing the average RSRP of all MDT samples positioned in each tile of the scenario, used by operators to detect coverage holes.
3) Error margin map: map showing the error margin of the average RSRP computed per tile, used to check the robustness of coverage level estimates. The error margin is computed per tile for a *Student's T*-distribution and 90% confidence level as

$$CI_{T-distribution} = \overline{RSRP} \pm t_{n-1}\frac{\sigma}{\sqrt{n}}\,, \qquad (2)$$

where $\overline{RSRP}$ is the average RSRP estimated per tile, σ is the standard deviation of RSRP measurements in the tile, n is the number of samples per tile, $n-1$ are the degrees of freedom and t is the value of *Student's T*-distribution depending on n and confidence level (90 % in this work).

The above-described maps are generated for the initial dataset (after removing duplicate MDT reports) and the filtered dataset containing only samples with valid positioning information. Maps are constructed with a 20-meter resolution. A 20*20m tile size is large enough to ensure that a significant share of tiles in populated areas have many MDT measurements, which reduces the uncertainty of signal level estimates derived by averaging samples per tile. At the same time, memory requirements are kept within reasonable limits when covering large geographical areas. Likewise, tile size is small enough to reduce spatial quantization error so as to capture large structures like blocks of building and motorways. Location accuracy threshold is fixed to the tile resolution (20 meters). For robustness, only tiles with more than 10 samples are considered in the analysis.

6.2 Results

6.2.1 Experiment 1 - Proof of concept

Fig. 6–(a) illustrates how the proposed algorithm classifies samples in trace 1 (dynamic UE). It is observed that the algorithm identifies 4 types of samples. First samples including accuracy information are classified as *convergent acquisition*. Then, the tracking phase is detected for the next minute. After that, thirty seconds of dead-reckoning starts, followed by a fixed location until confidence/uncertainty is reported again and the cycle restarts. As a result of filtering, 192 out of 1625 samples (i.e., 11.82 %) are defined as valid. Fig. 6–(b) maps the trace over an orthophoto. Markers are colored as in the legend of Fig. 6–(a). It is observed that all samples classified as convergent acquisition and tracking (blue and red markers) fall on the road, and are most likely valid. In contrast, dead reckoning and fixed samples fall outside the road, showing that those measurements are incorrectly located.

Fig. 7–(a) depicts the classification performed by the proposed algorithm in trace 2 (static UE). The figure shows how, after each period of rounded latitude, the algorithm classifies samples as *tracking* until completing a 1-minute interval. Then, it classifies samples as *deactivated* when no movement is detected, until movement is detected or a new period of rounded latitude or positioning accuracy reporting is detected. In this trace, only 125 out of 4375 samples are considered valid (i.e., a 2.86 %). Fig. 7–(b) maps the trace onto an orthophoto. It is observed that filtering has discarded many samples (grey markers) outside and inside the building, making it easier to determine the correct location of the UE.

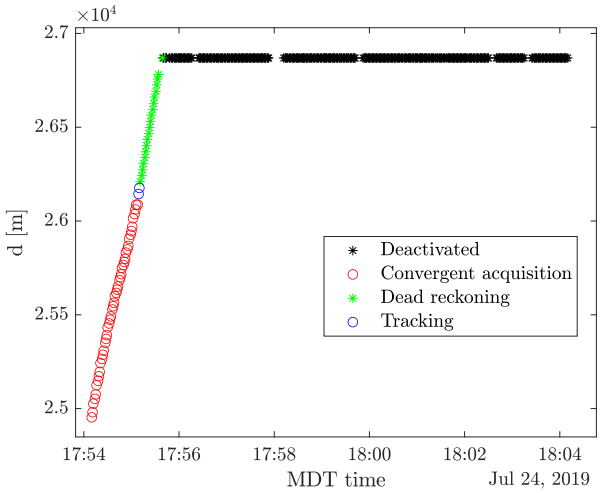

(a) Internal classification of the algorithm.

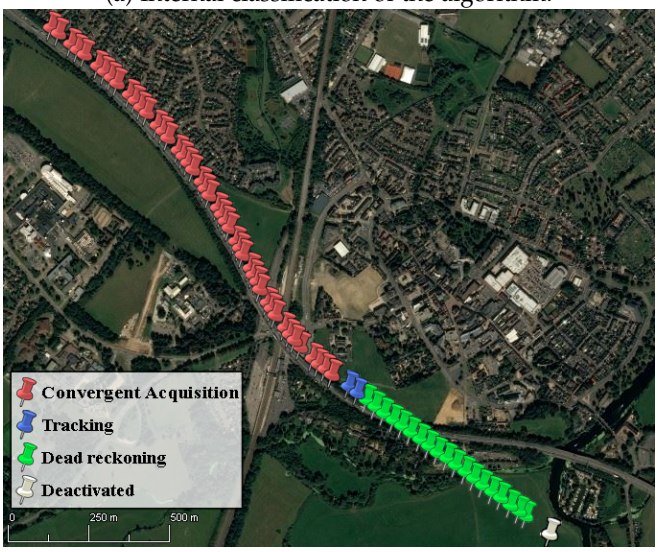

(b) Orthophoto.

Fig. 6: Graphical representation of the trace generated by a user traveling by car in a single period of 10 minutes (experiment 1 – dynamic UE).

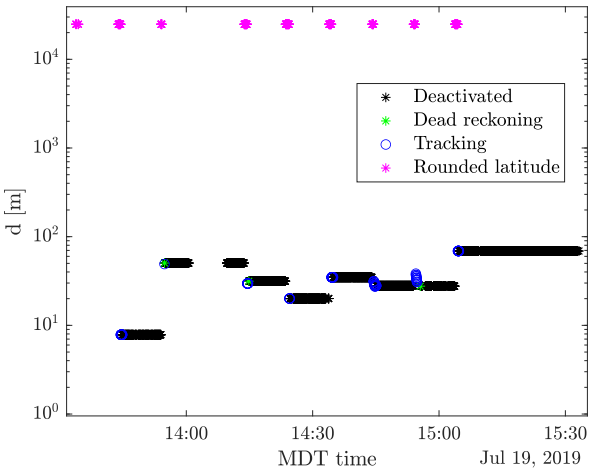

(a) Internal classification of the algorithm.

(b) Orthophoto (deleting rounded latitude positions).

Fig. 7: Graphical representation of the trace generated by a user inside an office building in the entire MDT report (experiment 2 – static UE).

6.2.2 *Experiment 2: Comparison of original and filtered maps*

The proposed algorithm detects 1 207 908 valid samples in the dataset (8.02 % of the samples available after removing duplicate MDT reports). To check the impact of filtering, Fig. 8–(a) and (b) show the density maps created with the original and filtered dataset, respectively. The number of samples is expressed in logarithmic units. It is observed that the aggressive filtering causes a significant decrease in the number of samples in most tiles. Specifically, the average number of samples per tile in the original and filtered maps is 519.38 and 41.72, respectively. Likewise, the number of tiles with more than 10 measurements in the original and filtered maps is 6437 and 2751, respectively. The impact on the latter indicators is clearly visible in the lower part of the figure, where it is observed how filtering eliminates many samples that fell out of the road in the original dataset.

Fig. 9–(a) and (b) depict the coverage maps obtained with the original and filtered dataset, respectively. For clarity, a georeferenced map of the scenario is overlapped. Triangular markers represent eNB positions and antenna azimuth, with the southernmost eNB being the one collecting MDT reports. By comparing RSRP levels in both maps, it is confirmed that the overall spatial distribution of coverage levels remains the same after filtering. Note that tiles with less than 10 samples after filtering are not represented in Fig. 9–(b). However, in the filtered dataset, the shape of roads and buildings can clearly be distinguished by suppressing samples in nearby green fields, where the probability of finding users is very low.

For a more detailed analysis, Fig. 10–(a) and (b) show a zoom of the coverage map in an area near the eNB collecting MDT traces before and after filtering, respectively. The figures cover an area of 4,4 ha with a mixture of indoor and outdoor zones, including a roundabout on the right and a set of buildings on the left, located a few hundred meters

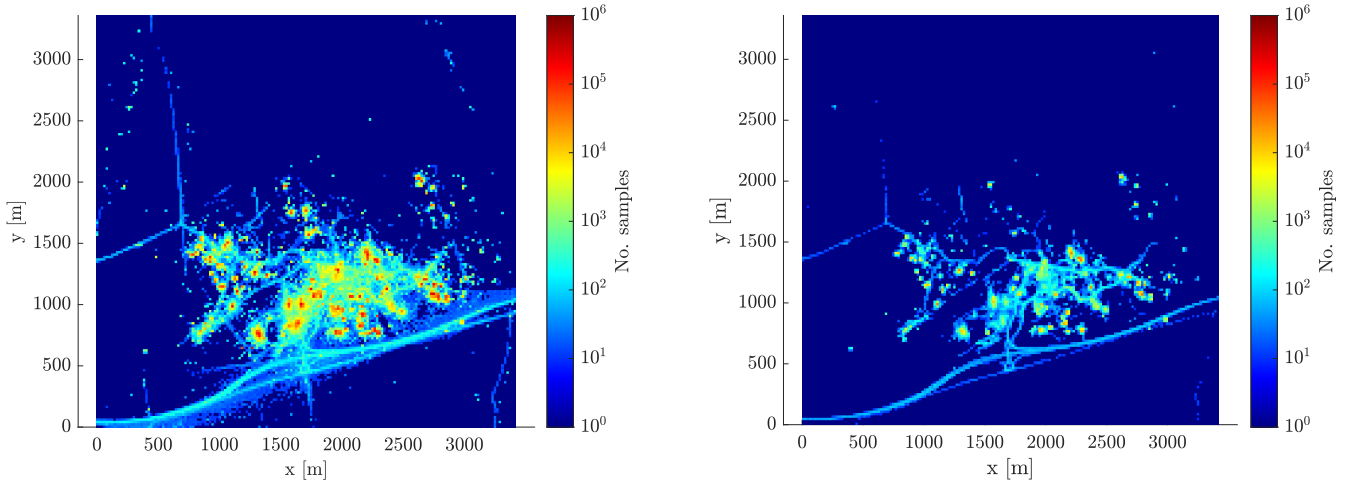

(a) Original dataset. (b) Filtered dataset.

Fig. 8: Density maps showing the number of samples per tile in logarithmic scale.

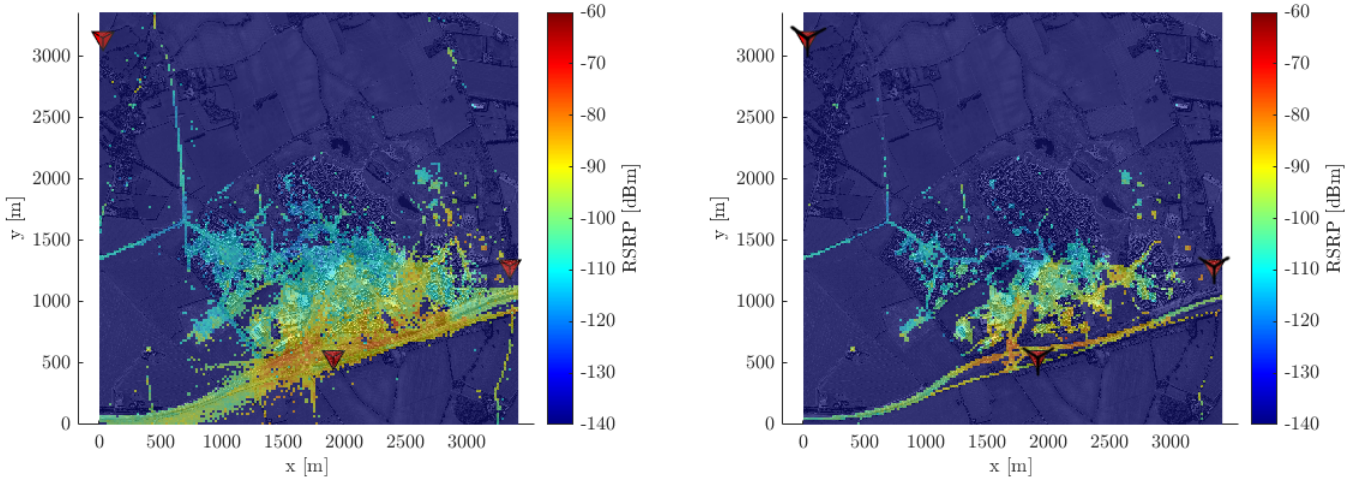

(a) Original dataset. (b) Filtered dataset.

Fig. 9: Coverage maps constructed by direct method (average RSRP per tile).

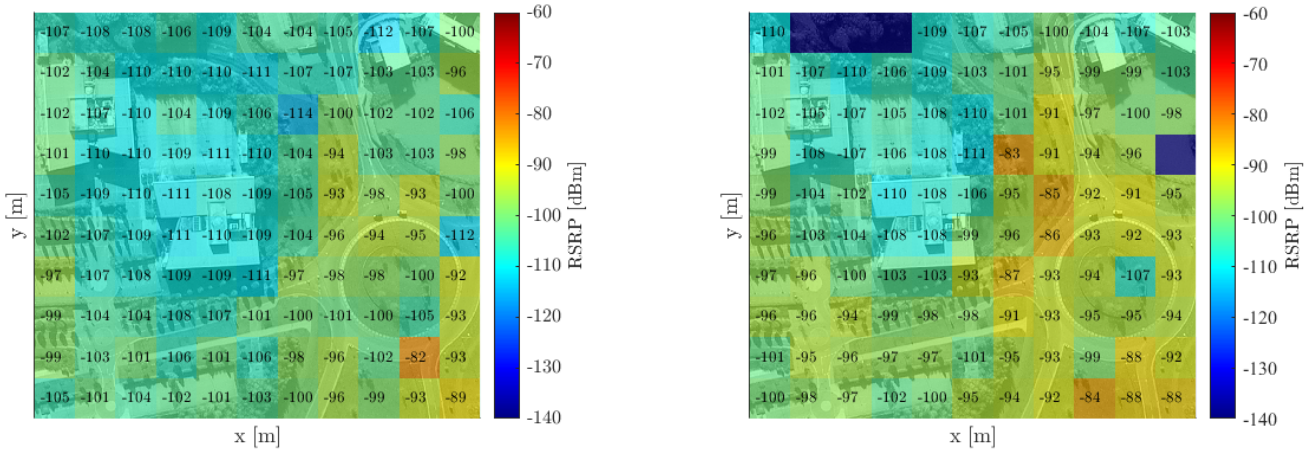

(a) Original dataset (b) Filtered dataset

Fig. 10: Coverage map in a zoomed area including indoor and outdoor environments.

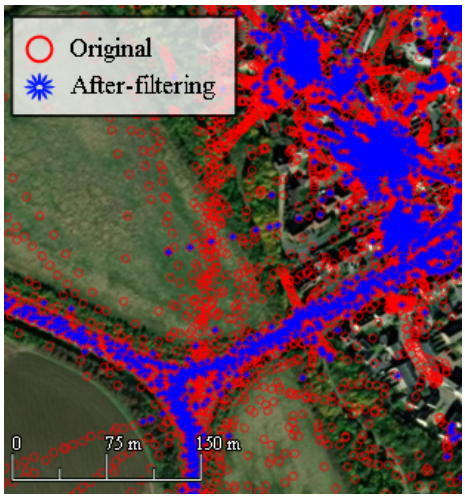

Fig. 11: Zoomed area of the scenario showing dead reckoning on roads and roundabouts (outdoor environment).

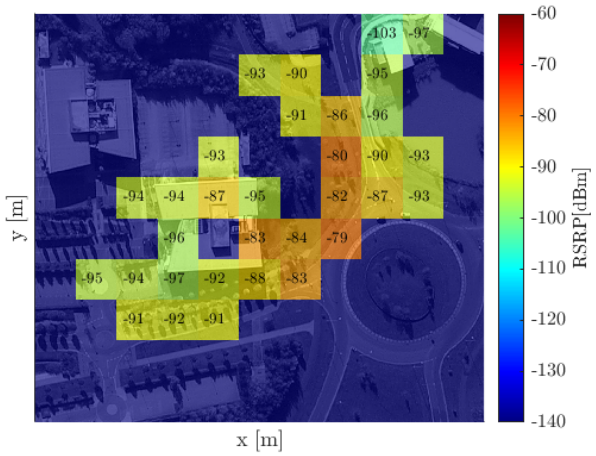

Fig. 12: Coverage map from MDT trace of a device under controlled test.

away from the eNB in line-of-sight conditions. Fig. 10–(a) shows that RSRP levels in the outdoor area surrounding the building (green area and road highlighted with a black square) range from -108 to -100 dBm, which are too low for the line-of-sight conditions and small distance to the eNB. Moreover, on the roundabout, contiguous tiles with abrupt changes in RSRP are observed (e.g., -82 dBm vs. -105 dBm). In contrast, in Fig. 10–(b), RSRP values in outdoor areas around the building are significantly higher (between -98 and -91 dBm), which are more consistent with the favorable propagation conditions. Furthermore, the above-mentioned abrupt changes of RSRP are smoothed out, showing more consistent results. A closer analysis shows that inconsistencies in the original map are mainly originated by dead reckoning periods, where UE trajectories are extrapolated in wrong directions (e.g., fast moving car inside a building) and static periods when a fixed latitude is reported for a moving user (e.g., user moving from indoors to outdoor or viceversa). Fig. 11 presents data samples belonging to several MDT traces collected near a roundabout. Blue stars and red circles represent location measurements before and after filtering, respectively. Original samples describe straights paths, suggesting that UEs in cars enter green fields (which has no sense). Such an undesirable effect is reduced after filtering.

To better check the consistency of coverage maps, an MDT trace is collected in an outdoor walk using a smartphone with GPS enabled to ensure that GPS is always in tracking mode. As the path runs through an open area, GPS noise should be much smaller than tile resolution (20 meters). Thus, the coverage map built with this trace can be considered as ground truth. RSRP values registered in the trace, depicted in Fig. 12, are compared to those in the same tiles in the original and filtered coverage maps. It is observed that values in the trace are closer to those in the map created with the filtered dataset (Fig. 10–(b)) than those in the original map (Fig. 10–(a)). Specifically, an average difference of 5 dB is computed in the former case, whereas a difference of 10 dB is computed in the latter case.

By filtering out inconsistencies, signal level deviations in each tile should be lower, resulting in more robust estimates of the average RSRP per tile. To check this statement, confidence intervals are calculated per tile with (2). Again, only those tiles with more than 10 samples are considered. Fig. 13–(a) present the cumulative density function of the standard deviation of RSRP per tile in the original and filtered map. Note that the filtered map has less tiles with measurements than the original map. For a fair comparison, both figures also break down the cumulative density function of the original map for tiles discarded and accepted by the filtering process (denoted as common and discarded tiles, respectively). From Fig. 13–(a), it can be inferred that the 3686 tiles in the original map left unpopulated by the filtering algorithm tend to have a larger standard deviation, as a result of wrongly located measurements. Moreover, the remaining 2751 tiles (common tiles) also show lower standard deviation in the filtered map.

The reduction in the number of samples per tile by filtering might jeopardize the reduction in standard deviation when computing RSRP averages per tile. Fig. 13–(b) presents the cumulative density function of the confidence margin per tile with the same break down as in Fig. 13–(a). It is observed that discarded tiles in the original map tend to have a large confidence margin, due to a larger standard deviation from incorrectly located measurements. Such a map clearance is one of the main benefits of the proposed algorithms. This is achieved at the expense of increasing confidence margins in the remaining tiles due to the lower number of samples. As a result, the 99th percentile of the confidence margin distribution is 1.1 dB lower after filtering (5.8 dB in the original dataset vs 4.7 dB in the filtered dataset). Thus, it can be concluded that filtering reduces large errors when estimating the average signal level per tile.

For a deeper analysis, Fig. 14 depicts a scatter plot of the 90% confidence margins in the original and filtered map. Each point in the figure represents a tile. Red and blue markers correspond to tiles in the original and filtered coverage map, respectively. It is observed that average confidence margins are consistently smaller in the filtered map, even

Pre-processing	Data filtering	Maps creation	Total
10.47 s	5.3 s	0.4 s	16.17 s

TABLE 2: Execution time of different stages in the algorithm (for 10 000 MDT reports).

when the latter has a lower number of samples per tile, n. From this observation, it is deduced that σ decreases due to the discarding of incorrectly geolocated measurements.

6.3 Computational efficiency

The proposed filtering algorithm requires pre-processing MDT reports and applying filtering rules. Its computational complexity grows linear with the number of reports in the dataset. Table 2 presents execution times of these stages in a laptop computer with an Intel i7-7700HQ CPU, 4 cores with 8 threads, a clock frequency of 2.8 GHz and 16 GB of RAM, when the algorithm is applied to the dataset described in Section 3.2. The time required to build coverage maps is also included, since it is one of the main uses of the algorithm. To ease comparison, run times are averages per 10 000 MDT reports. The total execution time takes 16.17 seconds per each 10 000 samples. The most time-consuming task is data pre-processing, comprising 65 % of the total execution time. The complexity of this task grows linear with the amount of available MDT samples. In the subsequent filtering phase, the main computational issue is to evaluate rules analyzing samples in a time window (i.e., detection of dead reckoning). The complexity of this task grows linear with the number of events (i.e., stages) per trace.

It should be pointed out that, the proposed filtering algorithm has to be executed whenever a new coverage map is derived, which is an infrequent task. Thus, execution time is not a critical issue. For other applications with real-time constraints, execution time can be reduced by restricting the temporal/spatial window of MDT data collection or parallelizing MDT trace filtering.

7 Conclusion

In current cellular systems, network replanning is one of the most critical task to avoid performance issues affecting user experience. For this purpose, MDT functionality provides geolocated information from UEs that can be used to create realistic and up-to-date coverage maps. A previous analysis of the dataset has allow to show with real measurements that positioning errors due to battery saving schemes severely limit the potential of MDT measurements for a wide range of scenarios. To circumvent this problem, a heuristic filtering algorithm has been proposed with generic and restrictive rules to discard samples with inaccurate location data. Method assessment has been carried out by checking the impact of filtering on the coverage map built with a real MDT dataset taken from a live LTE network in a suburban scenario. Results show that the proposed filtering method significantly improves the accuracy of coverage maps by eliminating unreliable measurements. Specifically, large errors margins are reduced by 1.1 dB, even if only 8% of samples are considered as valid.

The dataset used in this work comprises an MDT set collected in the network of a European tier-1 operator. The analyzed area is large enough to cover UEs with different mobility patterns (static, quasi-static and dynamic users), environments (indoor and outdoor) and land uses (roads, open areas, offices, residential, industrial, etc.). MDT features used as an input are defined by the 3GPP standard 37.320 [41], so current user equipment should be able to report them. Likewise, rules in the proposed filtering algorithm are generic, as they have been deduced by massive analysis of traces taken from a live network. For all these reasons, it is expected that the observations presented here can be extended to any cellular system. Nonetheless, it would be interesting to compare the behavior of different terminals (e.g., Android vs iOS) under different location settings (e.g., GPS-only vs WiFi-based). Obviously, terminals activating energy-saving modes less frequently will provide more accurate location information at the risk of introducing redundant information per tile. Unfortunately, such a detailed analysis requires information that can only be obtained by identifying users in massive datasets (which cannot be done for privacy reasons) or performing trials with selected terminals (which will never cover all the different situations in the live network). Note that the latter approach is complex, since not all handsets include MDT functionality (older models) and finding a particular user in an MDT dataset is extremely difficult (as C-RNTI changes). Future work will also check the impact of filtering in dense urban environments and higher frequency bands, where location accuracy is worse and propagation fluctuations are larger. It is envisaged that the benefit of filtering might be larger for these scenarios.

Acknowledgment

This work was funded by the European Union's Horizon 2020 research and innovation programme under the project H2020 LOCUS (Grant agreement no. 871249).

References

[1] F. Jejdling, P. Cerwall, P. Jonsson, S. Carson, R. Möller, *et al.*, "Ericsson mobility report," techreport, Ericsson, Nov. 2020.
[2] A. R. Mishra, *Advanced cellular network planning and optimisation: 2G/2.5G/3G... evolution to 4G*. John Wiley & Sons, 2007.
[3] F. Lehser, "A Deliverable by the NGMN Alliance NGMN Top OPE Recommendations," tech. rep., Sept. 2010.
[4] W. A. Hapsari, A. Umesh, M. Iwamura, M. Tomala, B. Gyula, and B. Sebire, "Minimization of drive tests solution in 3GPP," *IEEE Communications Magazine*, vol. 50, no. 6, pp. 28–36, 2012.
[5] J. Johansson, W. A. Hapsari, S. Kelley, and G. Bodog, "Minimization of drive tests in 3GPP release 11," *IEEE Communications Magazine*, vol. 50, no. 11, pp. 36–43, 2012.
[6] F. Diggelen, *A-GPS: Assisted GPS, GNSS, and SBAS*. 03 2009.
[7] D. Niculescu and B. Nath, "Ad hoc positioning system (APS) using AOA," in *IEEE INFOCOM 2003. Twenty-second Annual Joint Conference of the IEEE Computer and Communications Societies (IEEE Cat. No.03CH37428)*, vol. 3, pp. 1734–1743 vol.3, 2003.
[8] A. Vitaletti and E. Trevisani, "Cell-ID Location Technique, Limits and Benefits: An Experimental Study," in *Mobile Computing Systems and Applications, IEEE Workshop on*, (Los Alamitos, CA, USA), pp. 51–60, IEEE Computer Society, dec 2004.
[9] M. T. Simsim, N. M. Khan, R. Ramer, and P. B. Rapajic, "Time of arrival statistics in cellular environments," in *2006 IEEE 63rd Vehicular Technology Conference*, vol. 6, pp. 2666–2670, 2006.

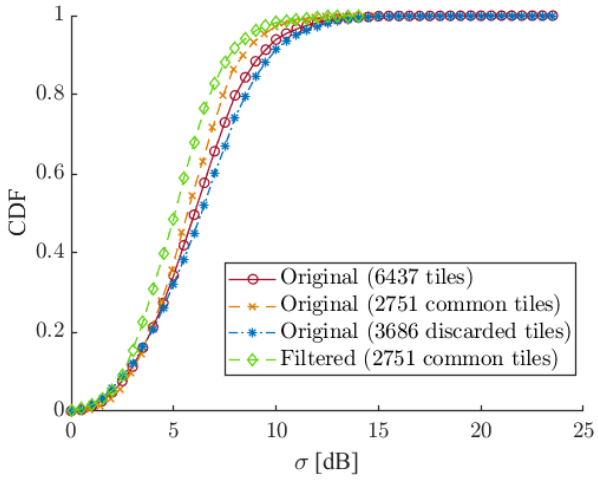

(a) CDF of standard deviation per tile.

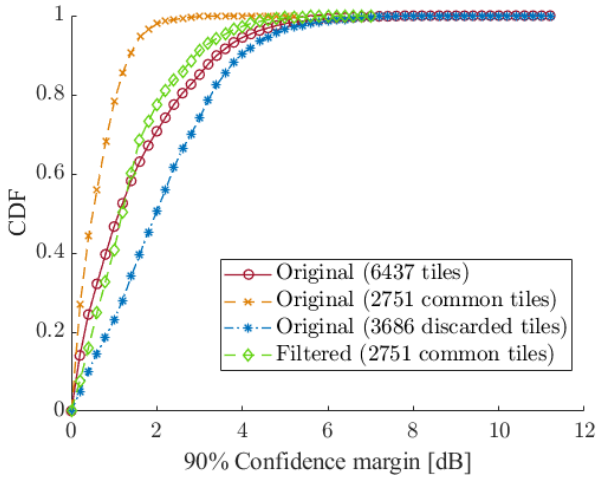

(b) CDF of confidence margin per tile.

Fig. 13: Cumulative distribution function of statistics per tile.

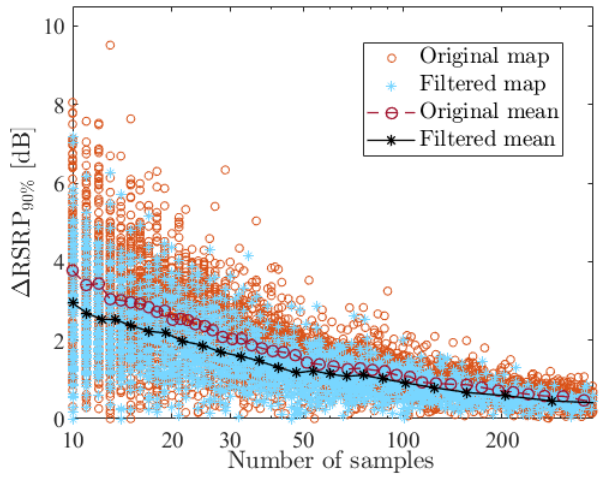

Fig. 14: Scatter plot with confidence margins depending on the number of measurements per tile (6437/2751 tiles).

[10] S. Fischer, "Observed time difference of arrival (OTDOA) positioning in 3GPP LTE," *Qualcomm White Pap*, vol. 1, no. 1, pp. 1–62, 2014.

[11] S. Frattasi and F. Della Rosa, eds., *Mobile Positioning and Tracking: From Conventional to Cooperative Techniques*. John Wiley & Sons, 2017.

[12] 3GPP, "TS 36.305, Stage 2 functional specification of UE positioning in E-UTRAN," Tech. Rep. Release 13, Versión 13.0.0, 3rd Generation Partnership Project, January 2016.

[13] Q. D. Vo and P. De, "A survey of fingerprint-based outdoor localization," *IEEE Communications Surveys Tutorials*, vol. 18, no. 1, pp. 491–506, 2016.

[14] S. Holm, "Hybrid ultrasound-RFID indoor positioning: Combining the best of both worlds," in *2009 IEEE International Conference on RFID*, pp. 155–162, 2009.

[15] P. D. Groves, "Navigation using inertial sensors," *IEEE Aerospace and Electronic Systems Magazine*, vol. 30, no. 2, pp. 42–69, 2015.

[16] F. Zafari, A. Gkelias, and K. K. Leung, "A survey of indoor localization systems and technologies," *IEEE Communications Surveys Tutorials*, vol. 21, no. 3, pp. 2568–2599, 2019.

[17] A. Dey, J. Hightower, E. de Lara, and N. Davies, "Location-based services," *IEEE Pervasive Computing*, vol. 9, no. 1, pp. 11–12, 2010.

[18] M. Kjærgaard, "Minimizing the power consumption of location-based services on mobile phones," *IEEE Pervasive Computing*, vol. 8, 01 2010.

[19] S. Garzon, M. Elbehery, B. Deva, and A. Küpper, "Reliable geofencing: Assisted configuration of proactive location-based services," pp. 204–207, 06 2016.

[20] D. Huber, "Background positioning for mobile devices-android vs . iphone," in *Joint Conference of IEEE Computer & Communication Societies*, 2011.

[21] P. Dabove, V. D. Pietra, and M. Piras, "Gnss positioning using mobile devices with the android operating system," *ISPRS International Journal of Geo-Information*, vol. 9, p. 220, 4 2020.

[22] L. L. Presti, J. I. Al-Azizi, and H. Z. M. Shafri, "Performance evaluation of pedestrian locations based on contemporary smartphones," *International Journal of Navigation and Observation*, vol. 2017, p. 6750346, 2017.

[23] M. Pesko, T. Javornik, A. Kosir, M. Stular, and M. Mohorcic, "Radio environment maps: The survey of construction methods," *KSII Transactions on Internet and Information Systems (TIIS)*, vol. 8, no. 11, pp. 3789–3809, 2014.

[24] M. Neuland, T. Kurner, and M. Amirijoo, "Influence of positioning error on X-map estimation in LTE," in *2011 IEEE 73rd Vehicular Technology Conference (VTC Spring)*, pp. 1–5, IEEE, 2011.

[25] M. A. Azpurua and K. Dos Ramos, "A comparison of spatial interpolation methods for estimation of average electromagnetic field magnitude," *Progress In Electromagnetics Research M*, vol. 14, pp. 135–145, 2010.

[26] D. Denkovski, V. Atanasovski, L. Gavrilovska, J. Riihijärvi, and P. Mähönen, "Reliability of a radio environment map: Case of spatial interpolation techniques," in *2012 7th International ICST Conference on Cognitive Radio Oriented Wireless Networks and Communications (CROWNCOM)*, pp. 248–253, 2012.

[27] L. Bolea, J. Perez-Romero, R. Agusti, and O. Sallent, "Context discovery mechanisms for cognitive radio," in *2011 IEEE 73rd Vehicular Technology Conference (VTC Spring)*, pp. 1–5, 2011.

[28] G. Mateos, J.-A. Bazerque, and G. B. Giannakis, "Spline-based spectrum cartography for cognitive radios," in *2009 Conference Record of the Forty-Third Asilomar Conference on Signals, Systems and Computers*, pp. 1025–1029, 2009.

[29] C. Phillips, M. Ton, D. Sicker, and D. Grunwald, "Practical radio environment mapping with geostatistics," in *2012 IEEE International Symposium on Dynamic Spectrum Access Networks*, pp. 422–433, 2012.

[30] G. Sun and J. Van de Beek, "Simple distributed interference source localization for radio environment mapping," in *2010 IFIP Wireless Days*, pp. 1–5, IEEE, 2010.

[31] H. B. Yilmaz and T. Tugcu, "Location estimation-based radio environment map construction in fading channels," *Wiley Wireless Communications and Mobile Computing, accepted*, 03 2013.

[32] I. Akbari, O. Onireti, M. A. Imran, A. Imran, and R. Tafazolli, "Effect of Inaccurate Position Estimation on Self-Organising Coverage

Estimation in Cellular Networks," in *European Wireless 2014; 20th European Wireless Conference*, pp. 1–5, 2014.
[33] I. Akbari, O. Onireti, A. Imran, M. A. Imran, and R. Tafazolli, "How reliable is MDT-based autonomous coverage estimation in the presence of user and BS positioning error?," *IEEE Wireless Communications Letters*, vol. 5, no. 2, pp. 196–199, 2016.
[34] H. N. Qureshi and A. Imran, "Optimal Bin Width for Autonomous Coverage Estimation Using MDT Reports in the Presence of User Positioning Error," *IEEE Communications Letters*, vol. 23, no. 4, pp. 716–719, 2019.
[35] A. Scaloni, P. Cirella, M. Sgheiz, R. Diamanti, and D. Micheli, "Multipath and Doppler Characterization of an Electromagnetic Environment by Massive MDT Measurements From 3G and 4G Mobile Terminals," *IEEE Access*, vol. 7, pp. 13024–13034, 2019.
[36] M. S. Grewal and A. P. Andrews, *Kalman filtering: Theory and Practice with MATLAB*. John Wiley & Sons, 2014.
[37] M. S. Arulampalam, S. Maskell, N. Gordon, and T. Clapp, "A tutorial on particle filters for online nonlinear/non-gaussian bayesian tracking," *IEEE Transactions on Signal Processing*, vol. 50, no. 2, pp. 174–188, 2002.
[38] Z. Li, K. Xu, H. Wang, Y. Zhao, X. Wang, and M. Shen, "Machine-learning-based positioning: A survey and future directions," *IEEE Network*, vol. 33, no. 3, pp. 96–101, 2019.
[39] J. Paek, J. Kim, and R. Govindan, "Energy-efficient rate-adaptive gps-based positioning for smartphones," in *Proceedings of the 8th International Conference on Mobile Systems, Applications, and Services*, MobiSys '10, (New York, NY, USA), p. 299–314, Association for Computing Machinery, 2010.
[40] D. Kim, S. Lee, and H. Bahn, "An energy-efficient positioning scheme for location-based services in a smartphone," in *2016 IEEE 22nd International Conference on Embedded and Real-Time Computing Systems and Applications (RTCSA)*, pp. 139–148, 2016.
[41] 3GPP, "TS 37.320, Technical Specification Group Radio Access Network; Universal Terrestrial Radio Access (UTRA), Evolved Universal Terrestrial Radio Access (E-UTRA) and Next Generation Radio Access; Radio measurement collection for Minimization of Drive Tests (MDT)," Tech. Rep. Release 16, Version 16.0.0, July 2020.
[42] 3GPP, "TS 32.422, Technical Specification Group Services and System Aspects; Telecommunication management; Subscriber and equipment trace; Trace control and configuration management," Tech. Rep. Release 16, Version 16.1.0, marzo 2020.
[43] N. Bui and J. Widmer, "Owl: a reliable online watcher for lte control channel measurements," 06 2016.
[44] 3GPP, "TS 23.032, Technical Specification Group Services and System Aspects; Universal Geographical Area Description (GAD)," Tech. Rep. Release 15, Version 16.0.0, Sept. 2018.
[45] J. Krumm, "Inference Attacks on Location Tracks," in *Pervasive Computing* (A. LaMarca, M. Langheinrich, and K. N. Truong, eds.), (Berlin, Heidelberg), pp. 127–143, Springer Berlin Heidelberg, 2007.
[46] R. Harle, "A survey of indoor inertial positioning systems for pedestrians," *IEEE Communications Surveys Tutorials*, vol. 15, no. 3, pp. 1281–1293, 2013.
[47] Sebastian Schweer, "Don't Worry: Google Only Checks Your Location Every 10 Minutes ." http://www.sastibe.de/2018/04/don-t-worry-google-location/, 2018. Online, Último acceso 24 de julio de 2020.
[48] M. Paonni, M. Anghileri, S. Wallner, J.-Á. Ávila-Rodríguez, and B. Eissfeller, "Performance assessment of GNSS signals in terms of time to first fix for cold, warm and hot start," *Institute of Navigation - International Technical Meeting 2010, ITM 2010*, vol. 2, pp. 1221–1236, Jan. 2010.
[49] W. McKinney, "Data Structures for Statistical Computing in Python," in *Proceedings of the 9th Python in Science Conference* (Stéfan van der Walt and Jarrod Millman, eds.), pp. 56 – 61, 2010.
[50] C. R. Harris, K. J. Millman, S. J. van der Walt, R. Gommers, P. Virtanen, D. Cournapeau, E. Wieser, J. Taylor, S. Berg, N. J. Smith, R. Kern, M. Picus, S. Hoyer, M. H. van Kerkwijk, M. Brett, A. Haldane, J. Fernández del Río, M. Wiebe, P. Peterson, P. Gérard-Marchant, K. Sheppard, T. Reddy, W. Weckesser, H. Abbasi, C. Gohlke, and T. E. Oliphant, "Array programming with NumPy," *Nature*, vol. 585, p. 357–362, 2020.
[51] I. The MathWorks, *Mapping Toolbox*. Natick, Massachusetts, United State, 2019.

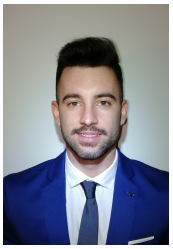

JOAQUÍN M. SÁNCHEZ-MARTÍN received his B.Sc. degree in Telecommunication Technologies Engineering and his M.Sc. double degree in Telecommunication Engineering and in Telematics and Telecommunication Networks from the University of Málaga, Spain, in 2017 and 2020, respectively. Currently, he is working working towards the Ph.D. degree. His research interests include optimization of radio resource management for mobile networks, location-based services, machine-learning and data analytics.

MATÍAS TORIL received his M.S. in Telecommunication Engineering and Ph.D. degrees from the University of Málaga, Spain, in 1995 and 2007, respectively. Since 1997, he is Lecturer in the Communications Engineering Department, University of Málaga, where he is currently Full Professor. He has co-authored more than 150 publications in leading conferences and journals and 8 patents owned by Nokia and Ericsson. His current re-search interests include self-organizing networks, radio resource management and data analytics.

VOLKER WILLE received the B.S. degree from the University of Applied Sciences and Arts of Hannover, Hannover, Germany, in 1991, and the Ph.D. degree from the University of Glamorgan, Cardiff, U.K., in 1995. He was an Intern with Bell Communications Research, Morristown, NJ, USA. He is currently with Nokia, Huntingdon, U.K., where he is involved in the optimization of cellular networks.

CAROLINA GIJÓN received her B.Sc. degree in Telecommunication Systems Engineering and her M.Sc. Degree in Telecommunication Engineering from the University of Málaga, Spain, in 2016 and 2018, respectively. Currently, she is working towards the Ph.D. degree. Her research interests include self-organizing networks, machine learning and radio resource management.

MARIANO FERNÁNDEZ-NAVARRO received his M.S. in Telecommunication Engineering from the Polytechnic University of Madrid in 1988 and the Ph.D. degree from the University of Málaga in 1999. He is on the staff of the Communications Engineering Department at the University of Málaga since 1992, after 3 years as design engineer at Fujitsu Spain S.A. His research interests include optimization of radio resource management for mobile networks and location-based services and management.